Analysis of the Stability of Looped-Out and Stacked-In Conformations of an Adenine Bulge in DNA Using a Continuum Model for Solvent and Ions

Martin Zacharias*# and Heinz Sklenar*

*Max Delbrück Center for Molecular Medicine, Theoretical Biophysics Group, and #Humboldt Universität Berlin, Institut für Biologie, D-10115 Berlin, Germany

ABSTRACT A combination of conformational search, energy minimization, and energetic evaluation using a continuum solvent treatment has been employed to study the stability of various conformations of the DNA fragment d(CGCAGAA)/d(TTCGCG) containing a single adenine bulge. The extra-helical (looped-out) bulge conformation derived from a published x-ray structure and intra-helical (stacked bulge base) model structures partially based on nuclear magnetic resonance (NMR) data were used as start structures for the conformational search. Solvent-dependent contributions to the stability of the conformations were calculated from the solvent exposed molecular surface area and by using the finite difference Poisson-Boltzmann approach. Three classes (I–III) of bulge conformations with calculated low energies can be distinguished. The lowest-energy conformations were found in class I, corresponding to structures with the bulge base stacked between flanking helices, and class II, composed of structures forming a triplet of the bulge base and a flanking base pair. All extra-helical bulge structures, forming class III, were found to be less stable compared with the lowest energy structures of class I and II. The results are consistent with NMR data on an adenine bulge in the same sequence context indicating an intra-helical or triplet bulge conformation in solution. Although the total energies and total electrostatic energies of the low-energy conformations show only relatively modest variations, the energetic contributions to the stability were found to vary significantly among the classes of bulge structures. All intra-helical bulge structures are stabilized by a more favorable Coulomb charge-charge interaction but destabilized by a larger electrostatic reaction field contribution compared with all extra-helical and most triplet bulge structures. Van der Waals packing interactions and nonpolar surface-area-dependent contributions appear to favor triplet class II structures and to a lesser degree also the intra-helical stacked bulge conformations. The large conformational variation found for class III conformers might add a favorable entropic contribution to the stability of the extra-helical bulge form.

INTRODUCTION

Bulges, extra unmatched contiguous nucleotides in an otherwise duplex helix, represent one of the most simple and common nonhelical structural elements in RNA and DNA. The presence of bulges in double-stranded DNA or RNA significantly reduces the electrophoretic mobility in polyacrylamide gels, indicating a bulge-induced bend of the double helix (Rice and Crothers, 1989; Battacharyya and Lilley, 1989; Battacharyya et al., 1990; Zacharias and Hagerman, 1995a). Electron microscopy (Hsieh and Griffith, 1989) and fluorescence energy transfer (FRET) studies (Gohlke et al., 1994) found a reduced end-to-end distance of bulge-containing DNA and RNA fragments compared with fully duplex fragments of the same length. For a series of adenine and uridine bulges in RNA the degree of bulge-induced bending has been quantified using transient electric birefringence (Zacharias and Hagerman, 1995a, 1997). Bend angles between ~10 and 20° for single-base bulges to up to ~90° for six-base bulges were found. RNA bulges may form ligand recognition motifs (Wu and Uhlenbeck, 1987) and can undergo large conformational changes upon ligand binding (Puglisi et al., 1992; Aboul-ela et al., 1995, 1996; Zacharias and Hagerman, 1995b). Most high-resolution structural studies have been performed on single-base bulges in DNA. A single unmatched adenine has been studied by x-ray crystallography (Miller et al., 1988; Joshua-Tor et al., 1988, 1992) and in a similar flanking sequence context by nuclear magnetic resonance (NMR) (Patel et al., 1982; Hare et al., 1986; Nikonowicz et al., 1989, 1990). The x-ray analysis revealed a looped-out (extra-helical) conformation with one adenine base partially stacked into the helix of the neighboring DNA molecule in the crystal whereas the NMR studies indicate an intra-helical conformation with the bulge base stacked between the flanking base pairs. Combinations of NMR spectroscopy and molecular modeling have also been applied to other single-base purine and pyrimidine bulges (Woodson and Crothers, 1988a,b, 1989; van der Hoogen et al., 1988a,b; Morden et al., 1983; Kalnik et al., 1989, 1990). The effects of flanking sequences, bulge base type, and temperature on the conformation of single-base DNA bulges has been studied by Kalnik and co-workers (1989, 1990). An important finding of these NMR studies is that in contrast to the x-ray structure single purine bulges appear to prefer the stacked, intra-helical conformation in solution independent of temperature (below the melting transition) and flanking sequence. However, small populations of extra-helical conformations could not be excluded in the NMR

Received for publication 30 June. 1997 and in final form 9 September. 1997.

Address reprint requests to Dr. Martin Zacharias, Max Delbrück Centrum Berlin, Robert Rössle Strasse 10, D-13122 Berlin, Germany. Tel.: 49-30-9406-3713; Fax: 49-30-9406-2548; E-mail: martin@iris2.biosim.mdc-berlin.de.

0006-3495/97/12/2990/14 $2.00

experiment (Hare et al., 1986). On the other hand, single pyrimidine bulges can adopt extra-helical as well as intra-helical conformations depending on sequence context and temperature (Kalnik et al., 1989, 1990).

The energetic contributions to the stability of the possible bulge conformations are not well understood. The aim of the present study was to analyze the energetic differences between a number of extra-helical and intra-helical forms of a single adenine bulge using a continuum approach for describing solvent effects. In this approach, DNA atoms and charges are explicitly taken into account whereas the aqueous environment and salt are represented as a continuum characterized by a solvent dielectric constant and a bulk salt concentration. For a given conformation of the molecule, the vacuum energy is defined by a sum of bond angle, torsion angle, and pairwise van der Waals and Coulomb electrostatic energy contributions. The process of transferring the solute from vacuum to water corresponds to an increase of the dielectric permittivity outside the molecule, resulting in a polarization of the dielectric medium, which in turn interacts with the charges of the molecule. This reaction field contribution to the energy of the system is also called electrostatic solvation free energy by analogy with the Born solvation free energy of spherical ions. If bulk ions are present, these rearrange according to a Boltzmann weighting of their energy in the field caused by the solute charges, adding a salt-dependent solvation contribution. For molecules of more complicated shape than spherical ions, the reaction field contributions can be calculated only numerically. For this purpose, the finite-difference Poisson-Boltzmann (FDPB) approach was employed in the present study. In addition to the charging process, transfer of a solute from vacuum to water leads to a reordering of water molecules at the interface between water and solute and, second, to van der Waals interactions between solute and water. Both latter contributions are assumed to be proportional to the solvent-accessible surface area of the solute with a proportionality constant γ (Sitkoff et al., 1994). The solvation contributions listed above include entropic solvent contributions and are, therefore, in principle, free energy contributions. The approach has been termed the FDPBγ approach and has been reviewed in detail by Honig et al. (1993) and Sitkoff et al. (1994). It yields the free energy of one conformation of a molecule in equilibrium with the surrounding solvent and ions. Configurational entropy contributions due to various molecule conformations are not accounted for. The mixing of an explicit atomic description of the solute and implicit description of the solvent assumes an instantaneous solvation of each solute structure. The approach principally neglects a possible dynamic coupling between solute conformational fluctuations and (possibly time-delayed) reactions of the solvent (mean field solvation model). Ion-ion correlation effects are neglected. There is also some uncertainty about the appropriate dielectric constant for the solute molecule (Smith et al., 1993; Yang et al., 1995). Although simulations using explicit solvent suggest a dielectric constant of 2–3 for the interior of DNA, larger values might be more appropriate for the polar surface regions (Yang et al. 1995). Nevertheless, within the approximations listed above, the FDPBγ approach offers a complete solvation description of a molecule (Honig et al., 1993).

It has been shown on a number of polar and nonpolar organic molecules that the FDPB approach is able to predict solvation free energies with similar accuracy as simulations using explicit solvent (Jean-Charles et al., 1991; Mohan et al., 1992; Sitkoff et al., 1994). The FDPB method has been used to characterize the energetics of peptide conformations (Yang and Honig, 1995a,b), electrostatic potentials around DNA (Jayaram et al., 1989), various DNA conformations (Friedman and Honig, 1992, 1995; Misra and Honig, 1996), and salt dependence of DNA-ligand complexes (Zacharias et al., 1992, Misra et al., 1994a,b; Fogolari et al., 1997) and, in combination with a conformational search, to analyze DNA-protein interactions (Zacharias et al., 1994) and protein loop conformations (Smith and Honig, 1994).

In the present study, the continuum solvent model has been applied to DNA model structures with six base pairs and a single central adenine bulge base. The model structures have been derived either from published x-ray coordinates (Joshua-Tor et al., 1988, 1992) or based on NMR data (Hare et al. 1986; Nikonowicz et al., 1989, 1990) or have been obtained from a conformational search. The intra-helical stacked adenine bulge form and a conformation with the adenine bulge base located in the DNA minor groove with the possibility to form a base triplet with a flanking G:C base pair were identified as the most stable bulge structures. Although the total free energy differences of the bulge in the intra-helical, triplet, and extra-helical conformations were found to be only 2.5–5 kcal mol^{-1}, the energetic contributions in terms of a decomposition into solvation and internal interaction contributions for each individual structure can differ by up to 20–40 kcal mol^{-1}. The results may have important implications for an understanding of structural transitions of bulge loop conformations in nucleic acids and for the mechanism of ligand binding.

MATERIALS AND METHODS

JUMNA algorithm

Conformational search and energy minimization have been carried out by means of the JUMNA (junction minimization of nucleic acids) program (Lavery, 1988; Lavery et al., 1995). The JUMNA algorithm was specifically designed to build, manipulate, and optimize nucleic acid structures. Special features of JUMNA arise from breaking down each nucleic acid strand into a series of 3′-monophosphate nucleotides. This enables one to use helical coordinates (three translations and three rotations) for positioning individual nucleotides in space, in combination with internal coordinates (dihedral angles and, within the sugar rings, valence angles) for describing the internal flexibility of each nucleotide (Sklenar et al., 1986; Lavery and Sklenar, 1988, 1989). In this way, not only a considerable reduction in the number of degrees of freedom, compared with the use of Cartesian coordinates, but also a versatile control over local and global characteristics of the structure is achieved. The junctions between successive nucleotides are closed using harmonic distance and valence angle

constraints during energy minimization. Bond lengths are assumed to be fixed at their optimal value.

In the current study on extra-helical and intra-helical bulge conformations, the JUMNA option of defining different helical axis systems for individual segments was used to perform molecular mechanics calculations under the condition that the base pairs adjacent to the bulge base are flanked by undistorted double-helical structures on either side. For this purpose, fixed nucleotide pairs (B-DNA caps) at the ends were linked to two different helical axis systems. Introducing a kink between the two axes leads to four additional degrees of freedom (two translations and two rotations). These kink variables allow for mutual rigid body motions of the caps and, consequently, for the full conformational freedom of the central bulge region and the two flanking base pairs.

Force field

The FLEX force field (Lavery et al., 1984, 1986) commonly used within JUMNA consists of the pairwise additive Coulomb type electrostatic and 6–12 dependent Lennard-Jones (LJ) potential terms complemented by harmonic valence angle terms and cosine dihedral barriers. In addition, an angle-dependent Lennard-Jones-type potential is used to deal with hydrogen bonds. In the present study, the calculation of free energy differences for solute-solvent interactions of different conformers was based on the continuum treatment of the solvent. This yields a sum of three terms including the electrostatic reaction field energy ΔG_{solv}, the nonpolar solvent-solute interaction ΔG_{SASA} (assumed to be proportional to the solvent-accessible surface area), and a salt-dependent term $\Delta\Delta G_{salt}$ (for a definition of these terms see below). The total conformational free energy was obtained by adding these terms to the intramolecular Coulomb, Lennard-Jones, and angle distortion energies defined by the FLEX force field and is given below:

$$\Delta G_{tot} = \Delta G_{solv} + \Delta G_{sasa} + \Delta\Delta G_{salt} + \sum(q_i q_j/(\epsilon_{in} R_{ij}) - A_{ij}/R_{ij}^6 + B_{ij}/R_{ij}^{12}) + \frac{1}{2}\sum V_s(1 \pm \cos(N_s \tau_s)) + \sum K_a(\sigma_a - \sigma_a^0)^2 \quad (1)$$

The partial charges q_i, the Lennard-Jones parameters A_{ij} and B_{ij}, and the parameters V_s, N_s, and K_a defining the distortion energy associated with torsion angle τ_s and valence angle σ_a, respectively, were taken from the FLEX parametrization. R_{ij} is the distance between atoms i and j, and ϵ_{in} denotes the dielectric permittivity in the solute volume. The additional Lennard-Jones-type potential used in FLEX to describe intramolecular hydrogen bonds was omitted. This term is inconsistent with the continuum model used in the present study as it favors only intramolecular hydrogen bonds and not possible hydrogen bonds of free donors and acceptors with water.

Note that this does not imply a zero strength of intramolecular hydrogen bonds as there are partial charges on hydrogen bond acceptor and donor atoms that still favor hydrogen bond formation.

The numerical treatment of the continuum model does not allow for including the first three terms of Eq. 1 in the conformational search and energy minimization by JUMNA. To enable comparison of free energies of different conformers, it is, however, important that each structure is at least close to a minimum of ΔG_{tot}. In the case of the bulge structures of this study, it turned out that ΔG_{SASA} and $\Delta\Delta G_{salt}$ depend only weakly on the conformation. Thus, in essence, it is the electrostatic model that has to be chosen in an appropriate way for performing the conformational search and energy minimization. For the system under study, we have observed a reasonable performance by using a simple pairwise Coulomb term with a constant dielectric permittivity of 4 in combination with a reduced phosphate group charge of −0.5. This choice results in a better correlation to the total electrostatic energy of the continuum treatment compared with the standard electrostatic term in JUMNA with a sigmoidal distance-dependent dielectric function (data not shown).

Solvent-accessible surface calculation

The solvent-accessible surface area (SASA) of each structure was calculated using the method by Shrake and Rupley (1973). A surface-area-dependent solvation term based on an analysis of the transfer free energy of hydrocarbons from vacuum to water (Sitkoff et al., 1994) was calculated using a linear relationship between SASA and nonelectrostatic (nonpolar) solvation free energy ($\Delta G_{SASA} = \gamma SASA + b$; $\gamma = 0.005$ kcal mol^{-1} Å^{-2}). The parameter γ has been obtained from a fit of the solvation free energy of a number of organic molecules versus SASA (Sitkoff et al., 1994). Parameter b is constant. As it is irrelevant when comparing ΔG_{SASA} for various conformers, it was set to zero. No surface curvature-dependent contributions have been considered.

Finite-difference Poisson-Boltzmann calculation

The University of Houston Brownian Dynamics (UHBD) program (Davis et al., 1991; Madura et al., 1995) was used for solving the FDPB equation and calculating electrostatic energies of NMR-based and x-ray-based model structures as well as a subset of structures obtained by the conformational search. Partial charges on each atom were taken from the FLEX force field. Atomic radii of 2.13 Å and 1.96 Å for sugar and aromatic carbon atoms, respectively, a radius of 1.68 Å for oxygen, 1.83 Å for nitrogen, 1.4 Å for hydrogen atoms at the sugars, and 1.25 Å for hydrogens at the bases were used. A surface dot density of 1000 points per atom and a solvent probe radius of 1.4 Å was used to define the solvent-inaccessible (interior) volume of the DNA molecule, which was assigned a dielectric permittivity, $\epsilon = 2.0$ (if not indicated otherwise). The solvent region of the box was assigned a dielectric permittivity $\epsilon = 78.0$. The dielectric boundary smoothing option was employed to reduce the grid dependence of the calculated electrostatic energies (Davis and McCammon, 1991).

The nonlinear Poisson-Boltzmann equation was solved to calculate salt-dependent contributions to the electrostatic solvation free energy (Luty et al., 1992). In this case, the electrostatic free energy was calculated using (Sharp and Honig, 1990)

$$\Delta G_{estat} = \int\left(\frac{q_f\varphi}{2} - \frac{q_m\varphi}{2} - \Delta\prod\right)dv$$

where q_f and q_m are the distributions of fixed and mobile (ionic) charges, respectively. The term Π denotes the osmotic pressure contribution due to the nonuniform distribution of ions in the electric field. The integral is over all grid points. Three-stage focusing calculations were performed starting with a 50^3 grid and a grid spacing of 2.5 Å, and the electrostatic potential from this calculation was used to calculate the boundaries for a 50^3 grid and 1.2 Å grid spacing. The calculated electrostatic reaction field energies are sensitive to the choice of grid parameters, in particular to the grid spacing used in the final grid. The dependence of the calculated solvation free energies on the grid spacing and on the orientation of the molecule relative to the grid was investigated for one bulge structure (see Fig. 1). As a compromise between numerical accuracy and computational demand, a grid spacing of 0.4 Å was used in the final grid (85^3 grid points). From Fig. 1, one can estimate a standard error on the order of kT (0.6 kcal mol^{-1} at room temperature) for this grid. Salt effects are much less sensitive to the grid parameters. All three grids fully encompassed each DNA structure. In the following, the total electrostatic free energy consists of a pairwise sum of the Coulomb interaction of all charged atom pairs (ΔG_{Coul}, $\epsilon = 2$) and a salt-independent reaction field contribution (ΔG_{solv}). The salt-dependent solvation free energy $\Delta\Delta G_{salt}$ of each structure is discussed separately and corresponds to the difference in electrostatic free energy at 150 mM monovalent and zero bulk salt concentration.

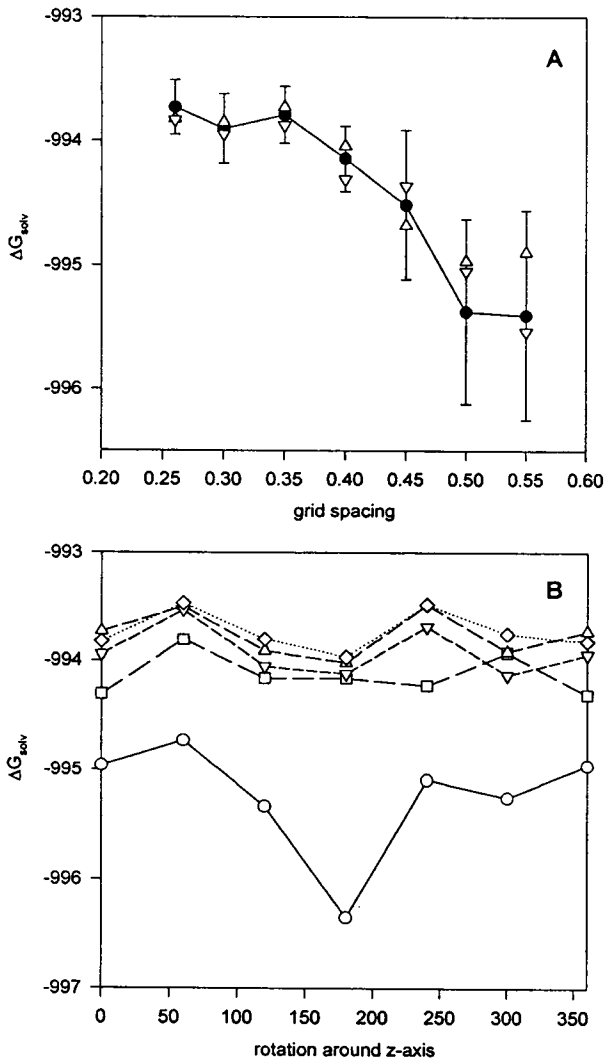

FIGURE 1 Grid dependence of FDPB electrostatic solvation free energies. The solvation (reaction field) free energy (ΔG_{solv}) of one bulge structure was calculated for various grid spacings and orientations of the final grid in the FDPB focusing calculations (three-step focusing calculation, see Materials and Methods). (*A*) For a given grid spacing, ΔG_{solv} for two positions of the molecule relative to the grid corresponding to shifts in all three Cartesian directions by half a grid spacing (△ and ▽) were calculated. In addition, the average solvation free energies for rotating the molecule in 60° steps around the helical axis are also displayed (●). The associated error bars indicate the standard deviation of ΔG_{solv} for rotation around the helical axis (in steps of 60°). (*B*) ΔG_{solv} is plotted versus orientation of the molecule relative to the grid with a grid spacing of 0.5 Å (○), 0.4 Å (□), 0.35 Å (▽), 0.3 Å (△), and 0.26 Å (◇), respectively. All calculations were performed with grids of approximately the same overall dimensions.

Bulge model structures

An extra-helical bulge conformation was generated using the atomic coordinates of the first six base pairs and the adenine bulge base from the tridecamer DNA x-ray structure, d(CGCAGAATTCGCG), with the adenine bulge base in bold (Joshua-Tor et al., 1988, 1992). This segment contains the bulge base at the center between double-stranded flanking sequences in a looped-out (extra-helical) conformation (dCGCAGAA/dTTCGCG). The helicoidal and backbone parameters describing this structure were calculated using the program CURVES (Lavery and Sklenar, 1988, 1989) and used as input for energy minimization using JUMNA.

A structural model for the intra-helical adenine bulge form of the same sequence was built starting from canonical B-form DNA for each nucleotide using JUMNA. The set of coordinates was used as starting coordinates for energy minimization yielding structure intra1. For the intra-helical bulge form, application of nuclear Overhauser enhancment (NOE) distance constraints, including 37 published distance constraints for a similar bulge sequence (d(CGCAGAGCTCGCG); Hare et al., 1986) between hydrogen atoms of the bulge base, and nearest and next-nearest neighbor base pairs lead to structure intra2 (no NOE distance constraints in the B-DNA caps of the structure have been included). The mean violation of NOE constraints was 0.17 Å, with a maximal violation of 0.5 Å. Note that the start structure for the constraint minimization intra1 fulfilled already 65% of the NOE distance constraints published by Hare et al. (1986) and violated all other distance constraints by <1.1 Å. Relaxation of the NOE distance constraints of structure intra2 resulted in structure intra3, with little deviation from intra2, indicating that the NOE constraints do not force any significant stereochemical perturbation. All energy minimization steps included B-DNA cap constraints (see above).

Conformational search procedure

Starting from the extra-helical (extra1) and intra-helical (intra1) bulge conformations, limited conformational searches were performed, changing systematically the sugar puckering of the bulge nucleotide and the two neighboring nucleotides. This scanning procedure consists of two energy minimization phases. In the first phase, the system is energy minimized, thereby constraining the corresponding sugars to a combination of preset pucker states. In a second phase, the pucker constraints were allowed to relax and the structure was minimized including only the B-DNA cap constraints described above for the two first and two last base pairs of the structure. Note that the second step of the procedure, relaxation without pucker constraint, can change the sugar pucker state and in general leads to a modification of other backbone and helical variables around the bulge site (for details, see Lavery et al., 1995). Six common sugar pucker states observed for DNA (Poncin et al., 1992; Lavery et al., 1995) were used in the structural scanning procedure (four C_2'-endo subforms, with pucker phases (*P*) of 178°, 168°, 157°, and 156°, respectively; one O_1'-endo constraint, $P = 90°$; and a C_3'-endo form, $P = 10°$, with pucker amplitudes between 35 and 42°).

RESULTS

Conformation of model structures based on x-ray and NMR data

Energy minimization of the x-ray adenine bulge structure (dCGCAGAA/dTTCGCG) yielded a structure, termed extra1, with a looped-out adenine bulge (Fig. 2). This energy-minimized structure shows a root-mean-square deviation (rmsd) from the start structure of 2.3 Å. The main effect of the energy minimization is an improved stacking of base pairs and a regularization of the x-ray DNA structure, in particular at the ends, due to the inclusion of B-DNA cap constraints. The desoxyriboses of all nucleotides of structure extra1 except for the bulge nucleotide are in the C_2'-endo form characteristic for canonical B-DNA. The bulge nucleotide sugar adopts the C_3'-exo form. The base pairs flanking the bulge stack on each other with very little overall curvature of the helical axis (<5°; Fig. 2 and Table 1). The inclusion of the B-DNA cap constraint at all modeling stages served to minimize end effects due to the short

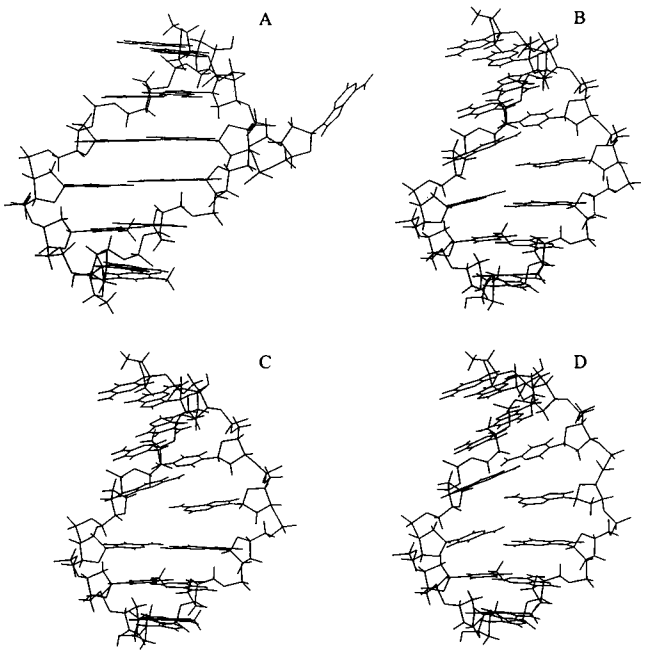

FIGURE 2 DNA bulge model structures (dCGCAGAA/dTTCGCG). The structure extra1 (*A*) was obtained by energy minimization of the first six base pairs and a central adenine bulge base of a published crystallographic structure (Joshua-Tor et al., 1992; see Materials and Methods). Energy minimization of a bulge-containing starting model with all nucleotides in canonical B-DNA conformation yielded intra1 (*B*). Applying NMR NOE distance constraints as published by Hare et al. (1986) resulted in structure intra2 (*C*), and relaxation of the NOE distance constraints yielded structure intra3 (*D*). The adenine bulge nucleotide 4 is located at the center of each structure (view into the minor groove).

length of the DNA fragment, embedding the bulge base and the flanking base pairs into the context of a B-DNA-type structure and to limit the conformational freedom of the bulge system. It is important to note that the present study, due to these constraints, principally neglects possible bulge-induced structural perturbations beyond the linkage of bulge flanking base pairs and next-nearest neighbor base pairs.

In contrast to the extra-helical form (extra1), all intra-helical model bulge structures cause a bending of the helical axis of ~20° (Fig. 2 and Table 1). The twist angle between the base pairs flanking the bulge nucleotide in the structures intra1–intra3 (~45°) is also larger than for extra1 (37°). All desoxyribose puckers of intra1–intra3 are in the C_2'-endo form. All base pairs in extra1 and intra1–intra3 show a Watson-Crick-type hydrogen-bonding network. However, in structures intra1 and intra3, the base pair G_5:C_{11} adjacent to the bulge is not perfectly planar. The C_{11} base is slightly tilted to fill the space due to the unmatched bulge base.

Comparing total energies of the two energy-minimized bulge model structures, extra1 and intra1, indicates a higher stability of the stacked form (intra1) by ~5 kcal mol^{-1} (Table 2). Similarly, the total energy of the intra-helical bulge structure, intra3 (relaxed intra2), is also by ~5 kcal mol^{-1} lower than the energy of extra1. The lower energy of the intra-helical forms is due to slightly more favorable van der Waals (ΔG_{LJ}), valence angle/torsion angle (ΔG_b), and total electrostatic free energy (ΔG_{Etot}). The energy difference between extra1 and intra2 is smaller. However, intra2 was obtained including more constraints (all NMR NOE distance constraints, see Materials and Methods) during the energy minimization compared with extra1 or the other intra-helical structures. The relatively small difference in total electrostatic energies is due to a compensation of solvation and pairwise Coulomb contributions. The electrostatic solvation free energies of the intra-helical forms are ~30 kcal mol^{-1} larger than the solvation free energy of the extra1 bulge structure. The favorable electrostatic solvation of extra1 is offset by an increased pairwise charge-charge interaction compared with the intra-helical structures (~33 kcal mol^{-1}). The salt contribution to the electrostatic solvation is very similar for all bulge structures, indicating that within the PB approach the electrostatic energy difference of different conformers is largely salt independent.

The nonpolar surface-area-dependent contribution ΔG_{SASA} stabilizes the intra-helical bulge conformations by ~0.4 kcal mol^{-1}.

Variation of partial charges and atomic radii in FDPB calculations

The electrostatic free energies calculated using the FDPB approach depend on the choice of atomic radii and partial charges on atoms of the solute. There is some uncertainty about the most useful set of partial charges and atomic radii for FDPB calculations (Sitkoff et al., 1994). To estimate the sensitivity of the results on the choice of these parameters, the electrostatic energies of the two bulge conformations, extra1 and intra3, were recalculated using various sets of atomic radii and partial charges. These calculations have served only to obtain an impression of the sensitivity of the results on the choice of these parameters; no systematic analysis has been performed. As shown in Table 3, using smaller radii and partial charges from the FLEX force field or charges from the optimal potentials for liquid simulations force field (Pranata et al., 1991) and the standard radii described in Materials and Methods reduces the electrostatic free energy difference ($\Delta\Delta G_{Etot}$) by 0.8 or 0.2 kcal mol^{-1}, respectively. The variations in the solvation and Coulomb contributions are slightly larger. As mentioned in the Introduction, there is also some debate about the appropriate dielectric constant of DNA (Yang et al., 1995). Raising the interior dielectric constant to $\epsilon = 6.0$ decreases the electrostatic free energy difference between both structures by ~0.6 kcal mol^{-1}. Both Coloumb ($\Delta\Delta G_{Coul}$) and solvation ($\Delta\Delta G_{solv}$) free energy differences are smaller than for an interior dielectric constant of $\epsilon = 2.0$. However, the conclusion derived in the previous paragraph that the extra-helical bulge form is stabilized by a more favorable electrostatic solvation and destabilized by an increased charge-charge repulsion holds in case of an increased interior dielectric constant as well as for all charge and radii modifications described above.

TABLE 1 Helical structure and NOE distance violations of selected low-energy bulge structures

Structure	Rise	Tilt	Roll	Twist	Curvature	NOE violation
extra1	3.3	0	1	38	3	1.2/4.2
intra1	4.9	12	−7	47	19	0.31/1.1
intra2	5.9	17	−2	46	18	0.17/0.55
intra3	4.9	15	−9	45	20	0.32/1.0
ClassI						
I-1	4.6	19	1.0	38	23	0.55/1.4
I-2	5.5	35	13	34	27	0.60/1.6
I-3	4.7	21	0	39	21	0.49/1.4
I-4	5.0	26	2	38	20	0.49/1.4
I-5	4.8	17	−15	37	18	0.61/1.65
I-6	4.4	20	6	41	27	0.51/1.45
I-7	4.7	18	1	39	27	0.40/1.4
ClassIIa						
IIa-1	3.0	5	−7	55	16	0.36/1.0
IIa-2	3.4	5	10	53	13	0.39/1.45
IIa-3	3.4	1	11	53	10	0.32/1.0
IIa-4	3.5	8	10	55	15	0.38/1.15
IIa-5	3.6	3	9	50	12	0.33/1.9
IIa-6	2.9	5	−1	56	17	0.49/1.9
ClassIIb						
IIb-1	3.7	12	−6	49	16	0.54/2.5
IIb-2	3.6	11	−4	46	14	0.66/2.5
ClassIII						
III-1	3.1	11	−7	37	6	1.3/4.9
III-2	3.0	5	−7	45	0	1.2/4.4
III-3	3.3	1	−10	41	2	1.1/4.1
III-4	3.3	2	4	25	11	1.3/5.6
III-5	3.0	8	3	36	6	0.9/3.0
III-6	3.0	4	−16	47	2	1.0/3.1
III-7	3.4	2	−2	42	4	0.75/2.8

The first column is classification of the bulge conformers. Columns 2–5 give the helical inter-base-pair parameters, rise (in Å), tilt, roll, and twist angles (in degrees), respectively, for base pairs flanking the bulge nucleotide. Column 6 gives the overall curvature defined by the angle (in degrees) between the helical axes associated with the B-DNA caps on either side of the structure using CURVES (Lavery and Sklenar, 1988, 1989). Column 7 is mean/maximal proton-proton distance violations from experimental NMR-derived proton-proton distances (Å) as published by Hare et al. (1986).

Interestingly, considering a model in which only the backbone (sugar and phosphate groups) of the DNA are charged (no partial charges on the bases) results in a total electrostatic free energy difference, electrostatic solvation, and Coulomb contributions very close to the values calculated for the fully charged DNA. Charging only the bulge base indicates a more favorable solvation in the extra-helical form. In contrast, charging all bases (no partial charges on the backbone) yields very similar solvation free energies for the two bulge forms. The unfavorable solvation of the bulge base in the stacked form appears to be partially compensated by a more favorable solvation of adjacent bases.

Conformational search

The x-ray structure might not necessarily correspond to the most favorable extra-helical bulge form in solution. In case of the intra-helical bulge conformer, the experimental NMR NOE distance constraints are not sufficient to define an accurate unique solution structure of the bulge. It is possible

TABLE 2 Energetic contributions to the stability of the adenine bulge (model start) structures

N	ΔG_b	ΔG_{LJ}	ΔG_{solv}	ΔG_{Coul}	ΔG_{Etot}	ΔG_{SASA}	ΔG_{tot}	$\Delta\Delta G_{salt}$
extra1	64.3	−54.8	−1029.8	−1754.1	−2783.9	14.8	−2759.6	−12.6
intra1	62.6	−55.7	−999.7	−1786.1	−2785.8	14.4	−2764.5	−12.4
intra2	62.5	−52.4	−1000.5	−1784.9	−2785.4	14.3	−2761.0	−12.5
intra3	63.9	−56.8	−998.2	−1787.9	−2786.1	14.4	−2764.6	−12.4

The first column indicates the type of the conformer (see text for details). Columns 2–9 are the free energy contributions in kcal mol^{-1} given in the following order: ΔG_b, valence and torsion angle contribution; ΔG_{LJ}, Lennard-Jones energy; ΔG_{solv}, electrostatic solvation (reaction field) free energy from a solution of the FDPB equation; ΔG_{Coul}, charge-charge (Coulomb) interaction energy ($\epsilon = 2$); ΔG_{Etot}, total electrostatic energy (sum of $\Delta G_{solv} + \Delta G_{Coul}$); ΔG_{SASA}, surface area contribution: $\Delta G_{SASA} = \gamma$SASA (SASA = solvent-accessible surface area in Å^2; $\gamma = 0.005$ kcal mol^{-1} Å $- 2$); ΔG_{tot}, total energy ($\Delta G_b + \Delta G_{LJ} + \Delta G_{Etot} + \Delta G_{SASA}$); $\Delta\Delta G_{salt}$, salt contribution to electrostatic solvation (difference of FDPB solvation free energy at 150 mM salt and zero salt).

TABLE 3 Electrostatic free energy differences of bulge structures for various sets of charges and atomic radii

	1	2	3	4	5	6	7
$\Delta\Delta G_{solv}$	−31.6	−9.7	−34.4	−32.4	−32.0	−0.7	−1.4
$\Delta\Delta G_{Coul}$	33.8	11.2	35.6	33.8	34.0	1.0	0.0
$\Delta\Delta G_{Etot}$	2.2	1.6	1.2	1.4	2.0	0.3	−1.4

$\Delta\Delta G_{solv}$, $\Delta\Delta G_{Coul}$, and $\Delta\Delta G_{Etot}$ correspond to the difference in electrostatic solvation and Coulomb and total electrostatic free energy (kcal mol^{-1}), respectively, of the two bulge structures extra1 and intra3. Column 1 shows the results for partial charges from the FLEX force field and standard atomic radii (see Materials and Methods); interior dielectric constant $\epsilon_s = 2.0$. Column 2 is the same as column 1 but using a solute dielectric constant $\epsilon_s = 6.0$ instead of $\epsilon_s = 2.0$. Column 3 is the same as column 1 but only charges on backbone (from FLEX force field), i.e., no charges on nucleobases, are used. Column 4 is the same as column 1, but smaller atom radii r_a are used; all r_a (carbon) = 1.7 Å, r_a (nitrogen) = 1.5 Å, r_a (oxygen) = 1.4 Å, r_a (hydrogen) = 1.0 Å, and r_a (phosphate) = 1.9 Å. Column 5 is the same as column 1, but charges and radii from the optimal potentials for liquid simulations force field (Pranata et al., 1991) are used. In column 6, only charges on nucleo-bases (from FLEX force field), i.e., no charges on backbone, are used. In column 7, only charges on bulge base (from FLEX force field) are used.

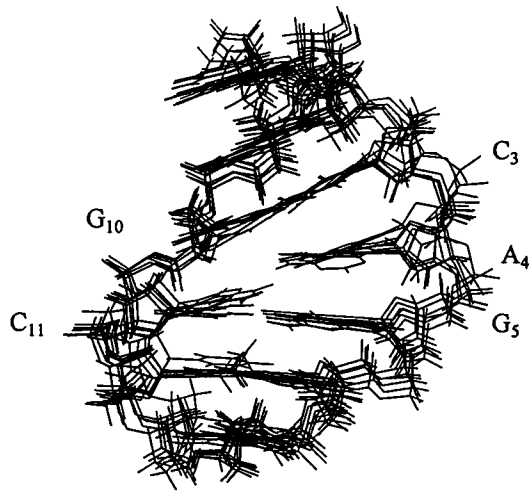

FIGURE 3 Superposition of class I bulge structures obtained by conformational search. The bulge structures I-1 to I-6, belonging to class I (stacked intrahelical bulge), are superimposed on the structure of lowest energy (I-1). The view is into the DNA minor groove. The positions of the bulge nucleotide (A_4) and flanking base pairs (C_3:G_{10}, G_5:C_{11}) are indicated.

that the results of the calculations on the bulge structures using a continuum solvent treatment are sensitive to the particular conformation used in the analysis. The aim of the conformational search is not to exhaustively search the conformational space available to the bulge structure but to limit the search to reasonable conformations starting from some of the model structures described above. The structural perturbation upon varying the desoxyribose pucker states of the nucleotides is less drastic than using the torsion angles at the phophodiester linkage between nucleotides as variables to generate starting conformations for the search. The two-phase procedure of first performing an energy minimization including the pucker constraints and subsequently relaxing the constraints in a second energy minimization usually also affects other nucleic acid backbone and helicoidal variables (often the optimal sugar pucker is reestablished with a corresponding change of backbone and helical variables). A subset of 40–50 conformers with energies not larger than 10 kcal mol^{-1} from the lowest energy structure of the generated ensemble were selected for a subsequent analysis using the FDPB approach.

Generated conformations were classified according to similar global conformational features. The low-energy conformations obtained starting from intra-helical bulge structures (in the following termed search 1) fall into at least two structural classes. Class I is an intral-helical bulge form, with the bulge base stacked in between the two flanking helices, very similar to the intra-helical start structures characterized also by a bulge-induced kink of the helix axis (Fig. 3 and Table 1). In the structures belonging to class IIa the adenine bulge neither completely stacks into the helix nor fully loops out but contacts the adjacent C_3:G_{10} base pair in the minor groove (triplet class; Figs. 4 and 5). A second type of triplet form (class IIb) was found with the bulge base located in the major groove in the same plane as the adjacent G_5:C_{11} base pair. Low-energy structures obtained from search 2, starting from the extra-helical bulge structure extra2, form class III. A common global feature of structures in class III is an almost straight helical geometry (average curvature of <10°; Fig. 6 and Table 1) and a large variation in the extrahelical bulge base position (for a more detailed structural characterization of classified bulge structures, see next paragraph). Other structures obtained from the conformational search are either not principally different

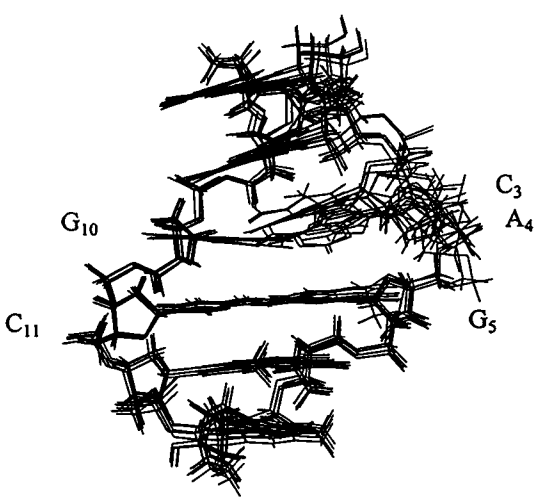

FIGURE 4 Superposition of class IIa bulge structures. The six lowest-energy bulge structures belonging to class II (triplet class) are shown superimposed on the lowest-energy class IIa structure (IIa-1). The structures were generated by a conformational search starting from structure intra1. The view is similar to the view in Fig. 3 (DNA minor groove). Bulge nucleotide (A_4) and flanking base pair (C_3:G_{10} and G_5:C_{11}) positions are indicated.

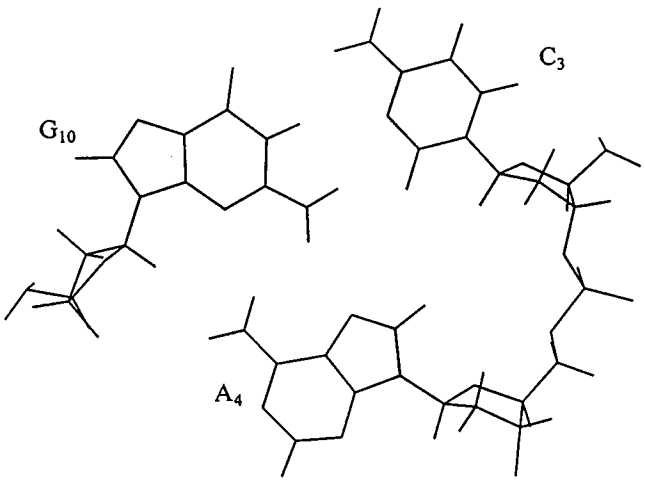

FIGURE 5 Arrangement of bulge nucleotide A_4 and the flanking C_3:G_{10} base pair in a low-energy triplet conformation (IIa-4), viewed along the helical axis.

from the structures of lowest energy (do not form a separate class) and/or are of much higher energy, unlikely to contribute to the Boltzmann ensemble of conformers in solution and will not be discussed in the following. All low-energy structures discussed below show a Watson-Crick-type base pairing of the base pairs adjacent to the bulge.

The calculated total energies of the low-energy conformers are ~5–8 kcal mol^{-1} lower than the total energy of the corresponding start structures, demonstrating that the search procedure can overcome barriers to identify new and lower-energy structures (Tables 2 and 4). The total energy of the lowest energy structure in class I is ~2.5 kcal mol^{-1} lower than the lowest energy of the extra-helical bulge forms (class III). The lowest-energy class II conformers are ~2.0 kcal mol^{-1} more stable than structures belonging to class III.

The total electrostatic energy (ΔG_{Etot}) of the lowest-energy intra-helical bulge structures is relatively constant and more favorable than the ΔG_{Etot} of the class II conformers but slightly larger than ΔG_{Etot} of the best extra-helical bulge structure. All extra-helical bulge forms are stabilized by a more favorable electrostatic solvation and destabilized by a larger Coulomb repulsion compared with the intra-helical and triplet bulge structures.

Most of the structures belonging to the triplet class (II) are intermediate between extra-helical and intra-helical forms in terms of solvation and Coulomb contributions to the electrostatic free energy. However, the structure of lowest energy within the triplet class (IIa-1) shows solvation and Coulomb contributions very similar to the intra-helical form. This structure is slightly different from other low-energy triplet forms (Fig. 3) in that the bulge base is slightly tilted relative to the adjacent C_3:G_{10} base pair and more buried than the bulge base in other triplet forms. The unfavorable total electrostatic energy of the class IIa,b bulge structures is balanced out by a more favorable Lennard-Jones packing interaction. Although the Lennard-Jones energy of the intra-helical and triplet forms is more favorable than in the case of fully looped-out conformers, there are some extra-helical bulge structures (e.g., the two lowest-energy structures III-1 and III-2) contacting the DNA in the major or minor groove with similar LJ energy as the intra-helical or triplet structures (Table 4).

The nonpolar surface area contribution as defined in the present study stabilizes the class IIa,b bulge conformers by ~0.5 kcal mol^{-1} compared with most class I and class III structures (except for those that show a bulge base contact in the minor or major DNA groove). The salt contributions to the solvation free energy are very similar for each structure, and the stability differences are largely salt independent.

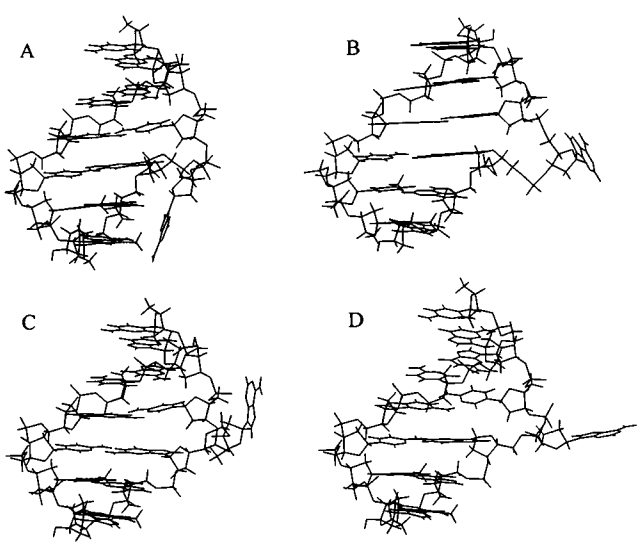

FIGURE 6 Comparison of four low-energy structures obtained from a conformational search starting from bulge structure extra1 (structures III-1, -3, -4, and -5).

Structural characterization

The average rmsd of the six structures, I-2 to I-7, from the structure of lowest energy in class I (I-1) was ~0.9 Å. Bulge conformers within class I are characterized by a bulge-induced kink of the helical axis of ~20° (Table 1). This kink is mainly caused by a large tilt of the base pairs flanking the bulge. The twist between base pairs adjacent to the bulge base can vary between 33° and 42°. The rise at the bulge site is larger compared with class II and III bulge structures due to the bulge base stacking between adjacent base pairs. The distance between the bulge phosphate group and adjacent phosphate groups (phosphate-phosphate distance) is similar to regular B-DNA (6–7.5 Å) for all class I conformers. Some of the class I conformers show a slight perturbation of the hydrogen-bonding network of the base pair (G_5:C_{11}) flanking the bulge with a tendency of the C_{11} base to tilt slightly toward the bulge base to fill the space between the flanking helices opposite to the bulge base

TABLE 4 Contributions to the stability of the adenine bulge structures (conformational search)

N	ΔG_b	ΔG_{LJ}	ΔG_{solv}	ΔG_{Coul}	ΔG_{Etot}	ΔG_{SASA}	ΔG_{tot}	$\Delta\Delta G_{salt}$
Class I								
I-1	63.4	−60.7	−1004.7	−1781.7	−2786.4	14.3	−2769.5	−12.4
I-2	64.0	−59.1	−999.1	−1787.5	−2786.7	14.4	−2767.7	−12.3
I-3	63.1	−58.5	−1000.6	−1785.8	−2786.4	14.3	−2767.4	−12.4
I-4	63.1	−58.4	−1000.9	−1785.4	−2786.3	14.3	−2767.2	−12.4
I-5	63.3	−58.5	−997.2	−1788.2	−2785.4	14.5	−2766.2	−12.4
I-6	64.3	−58.4	−998.4	−1787.9	−2786.4	14.5	−2766.0	−12.4
I-7	64.6	−58.0	−994.5	−1792.2	−2786.7	14.4	−2765.7	−12.3
Class IIa								
IIa-1	63.7	−62.3	−1002.4	−1782.3	−2784.7	14.0	−2769.2	−12.3
IIa-2	64.5	−64.2	−1014.0	−1768.4	−2782.4	13.7	−2768.5	−12.5
IIa-3	63.3	−65.1	−1019.0	−1761.0	−2780.0	13.7	−2768.2	−12.5
IIa-4	64.5	−62.6	−1010.0	−1772.5	−2782.5	13.9	−2766.6	−12.5
IIa-5	65.1	−63.4	−1015.0	−1766.7	−2781.7	14.0	−2766.1	−12.5
IIa-6	67.0	−62.1	−1013.2	−1771.4	−2784.7	14.0	−2766.0	−12.4
Class IIb								
IIb-1	65.0	−65.7	−1019.6	−1761.5	−2781.0	14.0	−2767.7	−12.4
IIb-2	66.0	−67.2	−1023.0	−1757.4	−2780.4	13.7	−2767.9	−12.4
Class III								
III-1	67.0	−64.9	−1035.5	−1747.8	−2783.4	13.9	−2767.3	−12.4
III-2	67.3	−64.0	−1032.5	−1751.5	−2784.0	14.0	−2766.7	−12.6
III-3	64.3	−55.8	−1028.7	−1757.7	−2786.4	14.9	−2763.1	−12.8
III-4	65.2	−59.6	−1027.9	−1754.7	−2782.6	14.3	−2762.7	−12.2
III-5	65.2	−56.3	−1017.4	−1768.4	−2785.8	14.7	−2762.2	−12.1
III-6	66.0	−63.0	−1030.0	−1749.9	−2779.9	13.6	−2763.2	−12.3

Energetic contributions are as given in the legend of Table 2. Class indicates the class the various structures belong to (see text). All energies are in kcal mol^{-1}.

(similar to structures intra1 and intra3). A smaller bulge-induced bending of the helical axis was observed for class IIa or class IIb conformers (Table 1). The twist between base pairs adjacent to the bulge base is significantly larger than for class I and class III conformers. The average rmsd of structures IIa-2 to IIa-5 from the structure of lowest energy within class II (IIa-1) was 1.1 Å.

A much broader variation of bulge conformations was observed for the low-energy extra-helical conformers. The average rmsd was 5.5 Å from structure III-1. In addition, a larger variation of the twist between base pairs flanking the bulge site (Table 1) was found compared with class I and II structures. For all low-energy extra-helical bulge conformers the phosphate-phosphate distance around the bulge site is smaller than for both the class I and class II structures (4.5–5.5 Å). This appears to be the primary structural reason for the enhanced Coulomb energy of these forms that, in combination with an increased solvent accessibility, counterbalances the more favorable solvation compared with intra-helical and triplet forms.

It is interesting to note that the backbone topology around the bulge site of structure III-3 (the structure of lowest energy in class III with a fully looped-out bulge base not contacting the DNA; see Fig. 6 *b*) is quite similar to the backbone topology of a recent adenine bulge structure in an RNA/DNA chimeric oligonucleotide (Portmann et al., 1996). This structure (in fact, two structures crystallized under slightly different conditions; Portmann et al., 1996) although in a different sequence context compared with the bulge x-ray structure of Joshua-Tor et al. (1992) and overall A-form, also shows the bulge base in a looped-out form. However, the sugar-phosphate backbone topology around the bulge of the Portmann et al. (1996) and Joshua et al. (1992) structures (or the current search 2 start structure extra1) differ significantly (>3 Å rmsd comparing the sugar-phosphate backbone of the bulge and neighboring nucleotides). Structure III-3 obtained as an alternative looped-out form after the conformational search has a corresponding rmsd (bulge and adjacent nucleotide backbone atoms) of ~0.9 Å from the Portmann et al. (1996) structure.

It is expected that extra-helical bulge conformers (class III) are compatible with a variety of backbone and sugar pucker states of the bulge nucleotide as there are fewer sterical limitations for the looped-out base than in the case of the stacked or triplet bulge forms. Interestingly, a number of different backbone torsion angle combinations of the bulge nucleotide and flanking bases appears to be compatible also with a low energy of the stacked base or the triplet bulge forms (see Table 5). The (torsion angle around O_5'-C_5' bond) and (C_3'-O_3') torsion angles were found to be relatively constant for all low-energy class I and II bulge conformers (*trans* configuration). Most variations were found for α (P-O_5'), γ (C_5'-C_4'), and ζ (O_3'-P) torsion angles (see Table 5). A number of class I and II structures showed an α-γ flip (a change in γ for one nucleotide around the bulge site (anti) correlates with a change in α in the previous nucleotide in the opposite direction). For all low-energy class II conformers, the torsion angle combination (*trans*, *gauche*, *-gauche*)

TABLE 5 Backbone structure of class I and class II bulge conformers

N	*P*	*A*	α2	α3	α4	γ3	γ4	γ5	ε3	ε4	ε5	ζ3	ζ4	ζ5
intra3	178	35	−75	−74	−67	58	59	66	−157	−170	−172	−147	−119	−127
Class I														
I-1	15	36	−84	−74	−63	53	60	75	−165	−174	−171	−73	−77	−126
I-2	19	37	−80	−73	168	54	61	−174	−168	−177	−171	−72	−71	−120
I-3	173	35	−85	−63	−66	53	67	62	−172	−170	−170	−83	−119	−130
I-4	172	36	−85	−62	−66	54	70	61	−172	−172	−170	−83	−116	−128
I-5	158	38	−79	172	−69	52	−173	60	−173	−166	−167	−83	−90	−136
I-6	161	40	−79	172	−134	53	−173	−179	−178	−160	−172	−85	−83	−124
I-7	3	35	−68	118	−62	55	−179	76	−158	−172	−171	−110	−79	−127
Class IIa														
IIa-1	197	39	157	64	−74	179	178	56	−88	−158	−171	−170	−77	−121
IIa-2	184	42	−62	46	139	64	−69	−178	−158	−168	−175	−174	−84	−114
IIa-3	151	43	−61	−70	135	66	51	−177	−158	−165	−173	−166	−85	−116
IIa-4	155	40	−61	139	123	65	−174	−172	−157	−159	−175	−176	−74	−116
IIa-5	153	46	−61	−74	145	63	50	180	−158	−174	−169	−162	−90	−94
IIa-6	2	35	154	119	−66	−179	−167	69	−156	−125	−174	−170	−57	−116

P and *A* correspond to sugar phase angle and sugar pucker amplitude, respectively, of the bulge nucleotide in the low-energy class I and class II bulge conformers and the bulge model structure intra3. DNA backbone torsion angles α*n* (around P-$O_{5'}$ bond), γ*n* ($C_{5'}$-$C_{4'}$), ε*n* ($C_{3'}$-$O_{3'}$), ζ*n* ($O_{3'}$-P) are given, with *n* indicating the nucleotide number (4 is the bulge nucleotide).

for the nucleotides 3, 4, and 5 (nucleotide 4 corresponds to the bulge nucleotide and 3 and 5 are adjacent nucleotides) was observed. In contrast, for most class I conformers, slightly larger ζ torsion angles (−70°–90°) in both nucleotides 3 and 4 were found compared with regular B-DNA (with ζ ~ −120°). Interestingly, the lowest-energy triplet bulge form includes a so-called B_{II} state at nucleotide 3. The difference between ε and ζ torsion angles has changed here from ~−90° as observed in regular B-DNA to ~90°.

The structures belonging to class I fulfill many of the published experimental NMR-NOE distance constraints (Hare et al., 1986; Nikonowicz et al., 1989), with mean and maximal distance violations of 0.4–0.6 and 1.4–1.6 Å, respectively (see Table 1). The mean and maximal NMR-NOE distance violations of conformers belonging to class IIa are even smaller compared with conformers of class I. A triplet bulge form as a possible solution conformation has also been suggested by Nikonowicz et al. (1989, 1990). It should be emphasized that the conformational search starting from intra1 was performed in the absence of any NMR-derived constraints. Nevertheless, the approach identified classes of low-energy conformers to a large degree compatible with experimentally determined NOE distance constraints. All extra-helical forms in class III appear to be incompatible with NMR results in that they violate several distance constraints by more than 4–5 Å (Table 1). Also, the structures in class IIb with the bulge base located in the major groove show a number of NOE distance violations of >2 Å.

DISCUSSION

Using a single-base adenine bulge in DNA as a model system, the aim of the current study was to identify energetic contributions to the stability of various bulge conformations within the framework of a continuum solvent model. A six-base-pair system was chosen because it allows for relatively accurate FDPB continuum electrostatic calculations. To evaluate the sensitivity of the results on the particular bulge conformations used in the analysis, a number of alternative conformers have been generated by a conformational search procedure. Structures of lower energy compared with the energy of the start structures, which were based on x-ray and partially on NMR data, could be identified. During the search an energy function with a more approximate electrostatic term than the FDPB electrostatic energy was used. To account at least partially for this inaccuracy, several structures below a certain energy threshold have been analyzed in more detail using the FDPB method. This approach of preselection of possible low-energy conformations of a molecule using an approximate energy function and subsequent more detailed analysis using more sophisticated approaches has been used in studies of peptide loop (Smith and Honig, 1994) and peptide turn (Yang and Honig, 1996) conformations and protein-DNA interaction (Zacharias et al., 1994).

Selected low-energy structures from the conformational search could be classified according to similar global conformational features. Besides structures with structural similarity to the start structures (class I and class III), an alternative low-energy bulge form with the adenine bulge base not fully looped out but located in the DNA minor groove and the possibility of forming a base triplet with the bulge flanking C_3:G_{10} base could be identified (class IIa). It is interesting to note that the same basic arrangement of three bases, termed a triad structure, has been suggested as a possible structural motif in DNA triplet repeat sequences by Kuryavyi and Jovin (1995). A triplet subclass could be distinguished with the bulge base contacting the DNA in the major groove (class IIb). The identification of bulge structures with a bulge-induced kink (classes I and II) as alternative low-energy bulge conformations in the present study

is consistent with the experimental results on bulge-induced helix bending, suggesting a bend angle of ~10–20° (Woodson and Crothers, 1988a,b, 1989; Rice and Crothers, 1989; Wang and Griffith, 1991; Zacharias and Hagerman, 1995a).

The calculated total energies of extra-helical bulge starting models based on a published x-ray structure (Joshua-Tor et al., 1988, 1992) and stacked forms, in part based on NMR data, differ by ~5 kcal mol^{-1} in favor of the intra-helical structure. Comparing lowest-energy extra-helical and intra-helical structures obtained from the conformational search resulted in 2.5 kcal mol^{-1} in favor of the intra-helical stacked bulge structure, slightly smaller than the energy difference found for the start structures. Note, however, that class III includes structures in which the bulge base contacts the DNA (see Fig. 6). Considering only the lowest-energy structures in class III with a fully solvent-exposed bulge base and no contacts of the bulge base and DNA (for example, III-3) the energetic difference compared with lowest-energy class I and II structures is larger (~5.5 kcal mol^{-1}). The lowest-energy triplet bulge forms appeared energetically almost as stable as intra-helical bulge conformers and slightly more stable than the lowest-energy extra-helical forms. This result is encouraging as NMR data have been found to be compatible with a stacked intra-helical or triplet adenine bulge form in solution (Hare et al., 1986; Nikonowicz et al., 1989, 1990; Kalnik et al., 1989). A possible reason as to why one adenine bulge in the crystal structure of Joshua-Tor et al. (1992) came out extra-helical might be intermolecular interactions with neighboring DNA molecules in the crystal. In fact, the looped-out adenine base in the crystal structure partially stacks into the neighboring DNA duplex (Joshua-Tor et al., 1992). These packing interactions are unlikely to occur in solution and might stabilize the looped-out form in the crystal.

The backbone topology around the bulge of one of the low-energy extra-helical bulge structures, III-3, was found to be similar to the corresponding region of an x-ray looped-out adenine bulge conformation of an RNA/DNA chimeric oligonucleotide (Portmann et al., 1996). This result supports the quality of the conformational search and energetic weighting using the present approach to extract alternative low-energy bulge structures within each class.

As has been demonstrated for a pair of extra- and intra-helical bulge model structures, variations in atomic radii or use of a different atom charge set can change $\Delta\Delta G_{Etot}$ by ~1 kcal mol^{-1}. The calculated total energy differences between the classes of bulge conformers (in particular, classes I and II) are not significantly larger than this force field sensitivity and the dependence of calculated electrostatic solvation energies on grid parameters (grid spacing and position of the DNA relative to the grid) in the FDPB calculations. This complicates an unambiguous identification of the lowest-energy bulge conformation within the present continuum model. The calculated energy differences of conformations within each class are in part also on the same order of magnitude as the inaccuracies of the FDPB method. Therefore, the order of low-energy conformers within each class given in Table 4 should be interpreted with care. However, these inaccuracies are small enough to justify the exclusion of bulge structures that are several kcal mol^{-1} higher in energy than the low-energy structures found in the present study and to collect and classify those structures with total energies within a threshold of the lowest-energy structure.

Interestingly, a number of distinct combinations of backbone torsion angles appeared to be compatible with the same global conformation even for class I and class II conformations with restricted conformational freedom of the bulge base. Again, the energetic differences between conformers in each class are not significantly larger than the numerical inaccuracies as discussed above. Definite conclusions about the relative population of these possible backbone substates cannot be made from the present study.

Although the accurate prediction of the total free energy difference of different conformers is important for an understanding of the stability of biological molecules, the identification of energetic factors or contributions that favor or disfavor certain classes of conformers might be as important for a characterization of driving forces, for example, of structural transitions in biological molecules.

In this regard, a major finding of the continuum model calculations is that all stacked bulge forms (class I), including the model start structures intra1–intra3, are electrostatically stabilized by a more favorable pairwise Coulomb interaction but disfavored by a reduced electrostatic solvation contribution compared with the extra-helical bulge structures (extra1 and all class III bulge structures) and to some degree also compared with the class II triplet bulge structures. It is important to emphasize that, in contrast to the total free energy difference of intra-helical and extra-helical bulge forms, the difference in electrostatic contributions as defined in the present study is significantly larger than the grid parameter and force field sensitivity of the FDPB results. Calculations on models with partial charges only on the DNA sugar-phosphate backbone indicated that the electrostatic effect is mainly due to differences in the DNA sugar-phosphate backbone of extra-helical and intra-helical bulge structures. The favorable electrostatic solvation of the bulge base alone in the extra-helical state is partially compensated by a more favorable solvation of adjacent bases in the intra-helical bulge structure compared with the extra-helical bulge form. The structural origin of the enhanced Coulomb repulsion in the case of the extra-helical model structures is primarily due to an accumulation of phosphate charges at the bulge site to allow base stacking of the bases flanking the looped-out bulge base. The salt dependence of the electrostatic free energies was similar for stacked and looped-out forms, indicating that the relative stability of the two forms is largely independent of the salt concentration. This, however, does not exclude the possibility of a preferential specific ion binding at, for example, a binding pocket formed between phosphate groups in case of the extra-helical bulge form compensating the charge-charge repulsion. In addition, as has been mentioned in the

Introduction, the Poisson-Boltzmann approach is limited due to the neglect of ion-ion correlation and ion-ion exclusion effects.

The van der Waals packing interactions were found to make a significant contribution to the stability of the various bulge conformations. The intra-helical stacked bulge form and the triplet class of bulge conformers are generally favored by packing interactions compared with the extra-helical bulge except for those extra-helical forms in which the bulge base contacts the DNA in the minor or major groove. As has been mentioned in the Introduction and Results, the surface-area-dependent contribution, ΔG_{SASA}, corresponds to the vacuum to water transfer of an organic molecule whereas the hydrophobic contribution is related to the transfer of a molecule from a nonpolar to an aqueous environment. The term ΔG_{SASA} includes not only unfavorable water ordering effects at the interface between solute and water but also favorable van der Waals interactions between solute and water molecules. Upon burying exposed solute surface, these favorable solute-solvent van der Waals interactions are partially compensated by improved solute-solute van der Waals interactions. Therefore, in the current formalism, part of the hydrophobic contribution is included in the favorable packing interaction in case of intra-helical and triplet bulge forms. Nonpolar contributions have also been found to make a favorable contribution to the stacking of bases in regular B-DNA (Friedman and Honig, 1992, 1995). Base stacking in regular B-DNA, however, corresponds to an optimal packing with very little unoccupied space between the bases. In contrast, stacking of a single base between two flanking helices in the case of the intra-helical bulge structure does not necessarily allow for an optimal van der Waals interaction.

The process of stacking a bulge base between flanking DNA helices has a lot in common with the process of ligand (bulge base) binding to a receptor (DNA). The current study demonstrates the importance of electrostatic solvation/desolvation contributions, which can largely compensate attractive Coulomb contributions. Poisson-Boltzmann studies on binding of ligands to DNA (Misra and Honig, 1995) or to proteins (Resat et al., 1997) have arrived at similar conclusions that attractive pairwise Coulomb interactions driving the association of receptor and ligand are often opposed by an electrostatic desolvation penalty of the partially charged atoms that become buried upon complex formation. Most current ligand-receptor docking attempts consider only the pairwise Coulomb contribution and are therefore likely to overemphasize attractive charge-charge interactions.

An interesting result of the current study is the observation that low-energy extra-helical forms (class III) show a much greater conformational variation than stacked (class I) and triplet forms (class II). To a certain degree, this is expected because stacking of the adenine base between the flanking helices restricts the conformational freedom of the bulge base. The greater conformational freedom of the extra-helical form might add a stabilizing entropic contribution. In this regard, the structural transition between the extra-helical bulge state and the intra-helical stacked or triplet state is similar to a transition between an unfolded (solvent-exposed, large conformational freedom) and folded (restricted conformational freedom, reduced solvent exposure) state of the bulge nucleotide. However, it is not clear whether the low-energy conformers found in the case of the extra-helical bulge structure correspond to narrow energy minima separated by high-energy barriers or whether the conformational space between these energy minima contains many other states of low energy similar to the conformations already characterized. An accurate estimation of the conformational entropy effect requires a much more comprehensive analysis of possible extra-helical forms beyond the scope of the present study.

The combination of conformational search, energy minimization, and energetic evaluation of minimized structures with a solvent continuum representation as used in the present form might not be comprehensive and accurate enough to unambiguously identify the bulge structure of lowest energy. However, the advantage is that, in contrast to explicit solvent simulations at a relatively modest computational cost, a large variety of conformations for a given structural motif can be generated and energetically evaluated. Although, in principle, more approximate than explicit solvent simulations, it accounts for solvation and ionic effects often neglected in molecular modeling studies of biomolecules. The approach appears to be useful to distinguish classes of low-energy structures for a given structural motif and to identify driving forces that stabilize or destabilize a certain structural class. Due to the limited accuracy and parameter dependence, it is difficult to identify the single most favorable conformation, but it is possible to achieve a restriction of the conformational space to regions of low energy within a given threshold. An encouraging result is that conformations that are in reasonable agreement with NMR data have been found as lowest-energy bulge structures. Other molecular modeling attempts neglecting solvation effects have been reported to fail in correlating agreement with NMR data and total energy of modeled conformers (Kajava and Rüterjans, 1993). This might offer the possibility of using the approach to assist in model building based on limited low-resolution NMR data of nucleic acid molecules.

M. Zacharias was supported by a DFG (Deutsche Forschungsgemeinschaft) Habilitation grant.

REFERENCES

Aboul-ela, F., J. Karn, and G. Varani. 1995. The structure of the human immunodeficiency virus type-1 TAR RNA reveals principles of RNA recognition by Tat protein. *J. Mol. Biol.* 253:313–332.

Aboul-ela, F., J. Karn, and G. Varani. 1996. Structure of HIV-1 TAR RNA in the absence of ligands reveals a novel conformation of the trinucleotide bulge. *Nucleic Acids Res.* 24:3974–3981.

Battacharyya, A., and D. M. J. Lilley. 1989. The contrasting structures of mismatched DNA sequences containing looped-out bases (bulges) and multiple mismatches (bubbles). *Nucleic Acids. Res.* 17:6821–6840.

Battacharyya, A., A. I. H. Murchie, and D. M. J. Lilley. 1990. RNA bulges and the helical periodicity of double stranded RNA. *Nature*. 343: 484–487.

Davis, M. E., J. D. Madura, B. A. Luty, and J. A. McCammon. 1991. Electrostatics and diffusion of molecules in solution: simulations with the University of Houston Brownian Dynamics program. *Comput. Phys. Commun.* 62:187–198.

Davis, M. E., and J. A. McCammon. 1991. Dielectric boundary smoothing in finite difference solutions of the Poisson equation: an approach to improve accuracy and convergence. *J. Comput. Chem.* 12:909–912.

Fogolari, F, A. H. Elcock, G. Esposito, P. Viglino, J. M. Briggs, and J. A. McCammon. 1997. Electrostatic effects in homeodomain-DNA interactions. *J. Mol. Biol.* 267:368–381.

Friedman, R. A., and B. Honig. 1992. The electrostatic contribution to DNA base-stacking interactions. *Biopolymers*. 32:145–159.

Friedman, R. A., and B. Honig. 1995. A free energy analysis of nucleic acid base stacking in aqueous solution. *Biophys. J.* 69:1528–1535.

Gohlke, C., A. I. H. Murchie, D. M. J. Lilley, and R. M. Clegg. 1994. Kinking of DNA and RNA helices by bulged nucleotides observed by fluorescence energy transfer. *Proc. Natl. Acad. Sci. USA*. 91: 11660–11664.

Hare, D., L. Shapiro, and D. J. Patel. 1986. Extra-helical adenosine stacks into right-handed DNA: solution conformation of the d(CGCA-GAGCTCGCG) duplex deduced from distance geometry analysis of nuclear Overhauser effect spectra. *Biochemistry*. 25:7456–7464.

Honig, B., K. A. Sharp, and A.-S. Yang. 1993. Macroscopic models of aqueous solutions: biological and chemical applications. *J. Phys. Chem.* 97:1101–1109.

Hsieh, C.-H., and J. D. Griffith. 1989. Deletions of bases in one strand of duplex DNA, in contrast to single-base mismatches, produce highly kinked molecules: possible relevance to the folding of single-stranded nucleic acids. *Proc. Natl. Acad. Sci. U.S.A.* 86:4833–4837.

Jayaram, B., K. A. Sharp, and B. Honig. 1989. The electrostatic potential of B-DNA. *Biopolymers*. 28:975–993.

Jean-Charles, A., A. Nicolls, K. A. Sharp A., B. Honig, B. Tempzyck, B. Hendrikson, and W. C. Still. 1991. Electrostatic contributions to solvation energies: comparison of free energy perturbation and continuum calculations. *J. Am. Chem. Soc.* 113:1454–1455.

Joshua-Tor, L., F. Frolow, E. Appela, H. Hope, D. Rabinovich, and J. L. Sussman. 1992. Three-dimensional structures of bulge-containing DNA fragments. *J. Mol. Biol.* 225:397–431.

Joshua-Tor, L., D. Rabinovich, H. Hope, F. Frolow, E. Appela, and J. L. Sussman. 1988. The three-dimensional structure of a DNA duplex containing looped-out bases. *Nature*. 334:82–84.

Kajava, A., and H. Rüterjans. 1993. Molecular modelling of the 3D structure of RNA tetraloops with different nucleotide sequences. *Nucleic Acids Res.* 21:4557–4562.

Kalnik, M. W., D. G. Norman, P. F. Swann, and D. J. Patel. 1990. Conformational transitions in thymidine bulge-containing deoxytridecanucleotide duplexes. *J. Biol. Chem.* 265:636–647.

Kalnik, M. W., D. G. Norman, M. G. Zagorski, P. F. Swann, and D. J. Patel. 1989. Conformational transitions in cytidine bulge-containing deoxytridecanucleotide duplexes: extra cytidine equilibrates between looped out (low temperatures) and stacked (elevated temperature) conformation in solution. *Biochemistry*. 28:294–303.

Kuryavyi, V. V., and T. M. Jovin. 1995. Triad DNA: a model for trinucleotide repeats. *Nature Genet.* 9:339–341.

Lavery, R. 1988. Junctions and bends in nucleic acids: a new theoretical modelling approach. *In* Structure and Expression. W. K. Olson, R. H. Sarma, M. H. Sarma, and M. Sundaralingam, editors. Adenine Press, New York. 121–211.

Lavery, R., and H. Sklenar. 1988. The definition of generalized helicoidal parameters and of axis curvature for irregular nucleic acids. *J. Biomol. Struct. Dyn.* 6:63–91.

Lavery, R., and H. Sklenar. 1989. Defining the structure of irregular nucleic acids: conventions and principles. *J. Biomol. Struct. Dyn.* 6: 655–667.

Lavery, R., H. Sklenar, K. Zakrzewska, and A. Pullman. 1986. The flexibility of nucleic acids. II. The calculation of internal energy and applications to mononucleotide repeats in DNA. *J. Biomol. Struct. Dyn.* 3:989–1014.

Lavery, R., K. Zakrzewska, and A. Pullman. 1984. Optimized monopole expansions for the representation of the electrostatic properties of the nucleic acids. *J. Comput. Chem.* 5:363–373.

Lavery, R., K. Zakrzewska, and H. Sklenar. 1995. JUMNA (junction minimization of nucleic acids). *Comput. Phys. Commun.* 91:135–158.

Luty, B. A., M. E. Davis, and J. A. McCammon. 1992. Solving the finite-difference non-linear Poisson-Boltzmann equation. *J. Comput. Chem.* 13:768–771.

Madura, J. D., M. E. Davis, R. Wade, B. A. Luty, A. Ilin, A. Antosiewicz, M. K. Gilson, B. Bagheri, L. Ridgway Scot, and J. A. McCammon. 1995. Electrostatics and diffusion of molecules in solution: simulations with the University of Houston Brownian Dynamics program. *Comput. Comm. Phys.* 91:57–95.

Miller, M., R. W. Harritson, A. Woldaver, E. Appela, and J. L. Sussman. 1988. Crystal structure of 15-mer DNA duplex containing unpaired bases. *Nature*. 334:85–86.

Misra, V. K., J. L. Hecht, K. A. Sharp, R. A. Friedman, and B. Honig. 1994b. Salt effects on protein-DNA interactions: the cI repressor and *Eco*RI endonuclease. *J. Mol. Biol.* 238:264–280.

Misra, V. K., and B. Honig. 1995. On the magnitude of electrostatic contribution to ligand-DNA interactions. *Proc. Natl. Acad. Sci. USA*. 92:4691–4695.

Misra, V. K., and B. Honig. 1996. Electrostatic contribution to the B to Z transition of DNA. *Biochemistry*. 35:1115–1124.

Misra, V. K., K. A. Sharp, R. A. Friedman, and B. Honig. 1994a. Salt effects on ligand-DNA binding: minor groove binding antibiotics. *J. Mol. Biol.* 238:245–263.

Mohan, V., M. E. Davis, J. A. McCammon, and B. M. Pettitt. 1992. Continuum model calculations of solvation free energies: accurate evaluation of electrostatic contributions. *J. Phys. Chem.* 96:428–6431.

Morden, K. M., Y. G. Chu, F. H. Martin, and I. Tinoco. 1983. Unpaired cytosine in the deoxyoligonucleotide duplex dCA_3CA_3G-dCT_6G is outside of the helix. *Biochemistry*. 22:5557–5563.

Nikonowicz, E., R. P. Meadows, and D. G. Gorenstein. 1990. NMR structural refinement of an extrahelical adenosine tridecamer d(CGCA-GAATTCGCG)$_2$ via a hybrid relaxation matrix procedure. *Biochemistry*. 29:4193–4204.

Nikonowicz, E., V. Roongta, C. R. Jones, and D. G. Gorenstein. 1989. Two-dimensional ^{1}H and ^{31}P NMR spectra and restrained molecular dynamics structure of an extra-helical adenosine tridecamer oligodeoxyribonucleotide. *Biochemistry*. 28:8714–8725.

Patel, D. J.,, S. A. Kozlowski L. A. Marky, J. Rice, C. Broka, K. Itakura, and K. J. Breslauer. 1982. Extra adenosine stacks into the self-complementary d(CGCAGAATTCGCG) duplex in solution. *Biochemistry*. 21:445–451.

Poncin, M., B. Hartmann, and R. Lavery. 1992. Conformational substates in B-DNA. *J. Mol. Biol.* 226:775–794.

Portmann, S., S. Grimm, C. Workman, N. Usman, and M. Egli. 1996. Crystal structures of an A-form duplex with single-adenosine bulges and conformational basis for site-specific RNA self-cleavage. *Chem. Biol.* 3:173–184.

Pranata, J. S. G., S. G. Wierschke, and W. L. Jorgensen. 1991. OPLS potential functions for nucleotide bases: relative association constants of hydrogen bonded pairs in chloroform. *J. Am. Chem. Soc.* 113: 2810–2819.

Puglisi, J. D., R. Tan, B. J. Calnan, A. D. Frankel, and J. R. Williamson. 1992. Conformation of the TAR RNA-arginine complex by NMR spectroscopy. *Science*. 257:76–80.

Resat, H., T. J. Marrone, and J. A. McCammon. 1997. Enzyme inhibitor association thermodynamics: explicit and continuum solvent studies. *Biophys. J.* 72:522–532.

Rice, J. A., and D. M. Crothers. 1989. DNA bending by the bulge defect. *Biochemistry*. 28:4512–4516.

Sharp, K. A., and B. Honig. 1990. Calculating total electrostatic energies with the nonlinear Poisson-Boltzmann equation. *J. Phys. Chem.* 94: 7684–7692.

Shrake, A., and J. A. Rupley. 1973. Environment and exposure to solvent of protein atoms: lysozyme and insulin. *J. Mol. Biol.* 79:351–365.

Sitkoff, D., K. A. Sharp, and B. Honig. 1994. Accurate calculation of hydration free energies using macroscopic solvent models. *J. Phys. Chem.* 98:1978–1988.

Sklenar, H., R. Lavery, and B. Pullman. 1986. The flexibility of nucleic acids. I. "SIR", a novel approach to the variation of polymer geometry in constraint systems. *J. Biomol. Struct. Dyn.* 3:967–987.

Smith, K. C., and B. Honig. 1994. Evaluation of the conformational free energies of loops in proteins. *Proteins Struct. Funct. Genet.* 18:119–132.

Smith, P. E., R. M. Brunne, A. E. Mark, and W. F. van Gunsteren. 1993. Dielectric properties of trypsin inhibitor and lysozyme calculated from molecular dynamics simulations. *J. Phys. Chem.* 97:2009–2014.

van den Hoogen, Y. T., A. A. van Beuzekom, H. van den Elst, G. A. van der Marel, J. H. van Boom, and C. Altona. 1988b. Extra thymidine stacks into the d(CTGGTGCGG)d(CCGCCCAG) duplex: an NMR and model building study. *Nucleic Acids Res.* 16:2971–2986.

van den Hoogen, Y. T., A. A. van Beuzekom, E. de Vroom, H. van den Elst, G. A. van der Marel, J. H. van Boom, and C. Altona. 1988a. Bulge-out structures in the single stranded trimer AUA and in the duplex (CUGGUGCGG)(CCGCCCAG): a model-building and NMR study. *Nucleic Acids Res.* 16:5013–5030.

Wang, Y. H., and J. Griffith. 1991. Effects of bulge composition and flanking sequence on the kinking of DNA by bulges. *Biochemistry.* 30:1358–1363.

Woodson, S. A., and D. M. Crothers. 1988a. Proton-nuclear magnetic resonance studies on bulge-containing DNA oligonucleotides from a mutational hot-spot sequence. *Biochemistry.* 26:904–912.

Woodson, S. A., and D. M Crothers. 1988b. Structural model for an oligonucleotide containing a bulged guanosine by NMR and energy minimization. *Biochemistry.* 27:3130–3141.

Woodson, S. A., and D. M. Crothers. 1989. Conformation of a bulge-containing oligomer from a hot spot sequence by NMR and energy minimization. *Biopolymers.* 28:1149–1177.

Wu, H.-N., and O. C. Uhlenbeck. 1987. Role of a bulged A residue in a specific RNA protein interaction. *Biochemistry.* 26:8221–8227.

Yang, A.-S., and B. Honig. 1995a. Free energy determinants of secondary structure formation. I. α-Helices. *J. Mol. Biol* 252:251–265.

Yang, A.-S., and B. Honig. 1995b. Free energy determinants of secondary structure formation. II. Anti-parallel β-sheets. *J. Mol. Biol.* 252: 366–376.

Yang, A.-S., and B. Honig. 1996. Free energy determinants of secondary structure formation. III. β-Turns and their role in protein folding. *J. Mol. Biol.* 259:873–882.

Yang, L., S. Weerasinghe, P. E. Smith, and B. M. Pettitt. 1995. Dielectric response of triplex DNA in ionic solution from simulations. *Biophys. J.* 69:1519–1527.

Zacharias, M., and P. J. Hagerman. 1995a. Bulge-Induced bends in RNA: quantification by transient electric birefringence. *J. Mol. Biol.* 247: 486–500.

Zacharias, M., and P. J. Hagerman. 1995b. The bend in RNA created by the trans-activation response element bulge of human immunodeficiency virus is straightened by arginine and by Tat-derived peptide. *Proc. Natl. Acad. Sci. USA.* 92:6052–6056.

Zacharias, M., and P. J. Hagerman. 1997. The influence of static and dynamic bends on the birefringence decay profiles of RNA helices: Brownian dynamics simulations. *Biophys. J.* 73:318–332.

Zacharias, M., B. A. Luty, M. E. Davis, and J. A. McCammon. 1992. Poisson-Boltzmann analysis of the λ-repressor-operator interaction. *Biophys. J.* 63:1280–1285.

Zacharias, M., B. A. Luty, M. E. Davis, and J. A. McCammon. 1994. Combined conformational search and finite-difference Poisson-Boltzmann approach for flexible docking. *J. Mol. Biol.* 238:455–465.